

# A universal DNA barcode for the Tree of Life

Bruno de Medeiros<sup>1,2,3</sup>, Liming Cai<sup>4,5</sup>, Peter J. Flynn<sup>4</sup>, Yujing Yan<sup>4</sup>, Xiaoshan Duan<sup>4,6</sup>,  
Lucas C. Marinho<sup>4,7</sup>, Christiane Anderson<sup>8</sup>, and Charles C. Davis<sup>4</sup>

<sup>1</sup>Field Museum of Natural History, Chicago, Illinois, 60605, USA

<sup>2</sup>Department of Organismic and Evolutionary Biology, Museum of Comparative Zoology,  
Harvard University, Cambridge, Massachusetts, 02138 USA

<sup>3</sup>Smithsonian Tropical Research Institute, Panama City, Panama

<sup>4</sup>Department of Organismic and Evolutionary Biology, Harvard University Herbaria,  
Harvard University, Cambridge, Massachusetts, 02138 USA

<sup>5</sup>Department of Integrative Biology, The University of Texas at Austin, Austin, Texas, 78712  
USA

<sup>6</sup>College of Forestry, Northwest Agriculture & Forestry University, Yangling 712100,  
Shaanxi, China

<sup>7</sup>Departamento de Biologia, Universidade Federal do Maranhão, Av. dos Portugueses 1966,  
Bacanga 65080-805, São Luís, Maranhão, Brazil

<sup>8</sup>University of Michigan Herbarium, 3600 Varsity Drive, Ann Arbor, Michigan 48108, USA

## Corresponding authors:

Bruno de Medeiros, Field Museum of Natural History, Chicago, IL, 60605; E-mail:

[bdemedeiros@fieldmuseum.org](mailto:bdemedeiros@fieldmuseum.org)

Charles C. Davis, Department of Organismic and Evolutionary Biology, Harvard University

Herbaria, Cambridge, MA 02138, USA; E-mail: [cdavis@oeb.harvard.edu](mailto:cdavis@oeb.harvard.edu)

## 27 **Abstract**

28 Species identification using DNA barcodes has revolutionized biodiversity sciences and  
29 society at large. However, conventional barcoding methods do not reflect genomic  
30 complexity, may lack sufficient variation, and rely on limited genomic loci that are not  
31 universal across the Tree of Life. Here, we develop a novel barcoding method that uses  
32 exceptionally low-coverage genome skim data to create a “varKode”, a two-dimensional  
33 image representing the genomic landscape of a species. Using these varKodes, we then  
34 train neural networks for precise taxonomic identification. Applying an expertly annotated  
35 genomic dataset including hundreds of newly sequenced genomic samples from the plant  
36 clade Malpighiales, we demonstrate >91% precision when identifying species or genera.  
37 Remarkably, high accuracy remains despite minimal data amounts that lead to failure when  
38 applying alternative methods. We further illustrate the broad utility of varKodes across  
39 several focal clades of eukaryotes and prokaryotes. As a final test, we classify the entire  
40 NCBI eukaryote sequence-read archive to identify its 861 constituent families with >95%  
41 precision despite utilizing less than 10 Mbp of data per sample. Enhanced computational  
42 efficiency and scalability, minimal data inputs robust to degraded DNA, and modularity for  
43 further development make varKoding an ideal approach for biodiversity science.

44  
45 **Keywords:** biodiversity science, computer vision, DNA barcoding, Malpighiaceae, natural  
46 history collections, neural networks, species identification, taxonomy

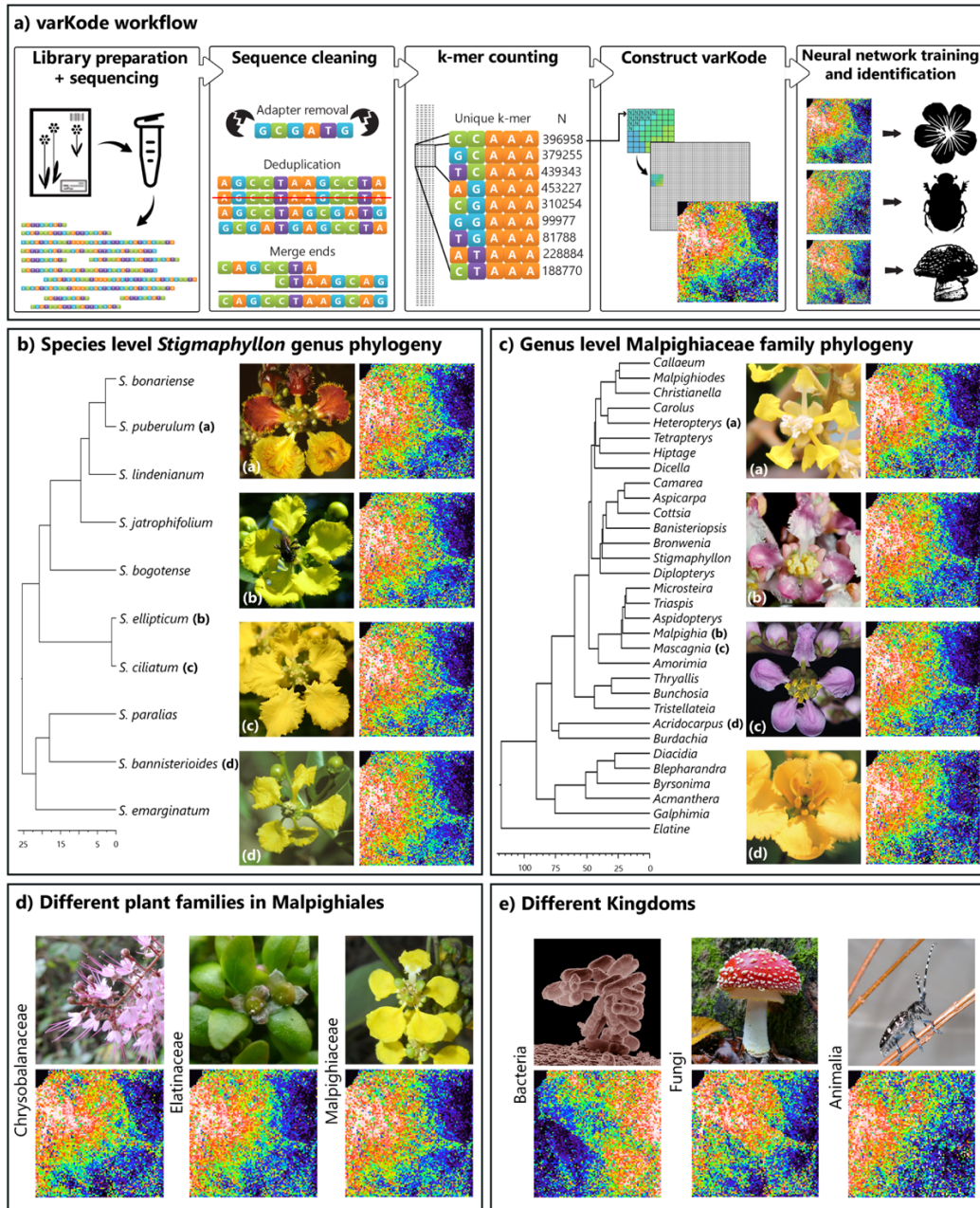
# 47 Introduction

48 For two decades, conventional DNA barcoding, which relies on standardized short  
49 sequences (400–800 bp) for species identification<sup>1, 2, 3, 4, 5</sup>, has enabled novel and massively  
50 scalable science spanning evolution<sup>4, 6, 7, 8, 9</sup>; ecology<sup>10, 11, 12, 13, 14</sup> and paleontology<sup>15, 16, 17, 18,</sup>  
51 <sup>19</sup>. Practical applications of barcoding have also made major contributions to  
52 environmental health, including the ability to authenticate medicinal plants<sup>20</sup>, detect  
53 agricultural pests<sup>21</sup>, and monitor poaching and the trade of endangered species<sup>22, 23, 24, 25, 26,</sup>  
54 <sup>27</sup>. Despite these remarkable achievements, however, conventional DNA barcoding suffers  
55 from at least four limitations. First, barcodes are customized specifically for particular  
56 clades of organisms (e.g., plants, animals, and fungi), and therefore are not universal—in  
57 many cases even within focal clades. For example, commonly used plant barcodes from  
58 chloroplast genes such as *matK* and *rbcL* cannot be applied as barcodes for all plants<sup>28, 29</sup>,  
59 or for animals and fungi. Second, conventional barcode loci may fail to distinguish closely  
60 related taxa, a pervasive shortcoming in plants<sup>2, 30</sup>. Third, reliance on a single locus may  
61 lead to spurious results in the case of complex evolutionary scenarios such as hybridization  
62 in deep and shallow time<sup>31, 32, 33, 34</sup>. And fourth, the necessary comparison of homologous  
63 genes may fail when PCR primers are not universal<sup>35</sup>, the source DNA is fragmented<sup>27</sup>, or  
64 paralogy and the presence of pseudogenes confounds accurate orthology assessments<sup>36, 37</sup>.  
65  
66 Newer alternatives to conventional barcoding have begun to address these challenges by  
67 leveraging two technological advancements: high-throughput sequencing and machine-  
68 learning applications powered by neural networks. High-throughput sequencing facilitates  
69 more comprehensive assessments of total genomic space<sup>38, 39</sup>. For example,  
70 presence/absence patterns among short DNA sequences (k-mers) from low-coverage reads  
71 (i.e., genome skims) can estimate overall sequence distances, bypassing genome alignments  
72 entirely as implemented in *Skmer*<sup>40</sup>. Machine learning enables more complex sequence  
73 comparisons than do more conventional methods that rely on homology and simple  
74 metrics<sup>41</sup>. Machine-learning models can cluster DNA sequences correctly without  
75 supervision<sup>42, 43</sup> and can classify sequences based on reference datasets<sup>44, 45, 46, 47</sup>. In

76 particular, neural networks are exceptionally powerful for sophisticated computer-vision  
77 tasks, such as image classification<sup>48</sup>. Thus, the combination of low-coverage genome  
78 skimming data and neural networks holds enormous promise for accurate and scalable  
79 DNA barcoding, but its potential has yet to be fully realized.

80

81 Genomes differ substantially in many features beyond the simple nucleotide differences  
82 commonly used in conventional barcoding (e.g., repeat content), but these differences have  
83 been overlooked for species identification<sup>49, 50, 51, 52</sup>. We propose that i.) relevant genomic  
84 features can be captured by nucleotide composition with short k-mer counts and very  
85 small sequence coverage; and ii.) these counts can be used to distinguish species and  
86 higher taxa efficiently and accurately using machine learning. Inspired by prior work<sup>42, 44,</sup>  
87 <sup>53</sup>, we developed a novel barcoding method (**varKoding**) that integrates genome skim data  
88 with machine-learning models trained using two-dimensional images representing genome  
89 composition (a **varKode**) (**Figure 1A**). To assess the utility of varKoding for accurate  
90 species identification, we first generated a *de novo* genome skim dataset including  
91 hundreds of samples derived primarily from historical herbarium specimens for the  
92 diverse plant genus *Stigmaphyllon* (Malpighiaceae), which has received extensive  
93 phylogenetic and taxonomic treatment<sup>54, 55, 56, 57, 58</sup>. Upon establishing the power and  
94 robustness of our tool for identifying species of *Stigmaphyllon*, we explored the utility of  
95 varKodes at greater phylogenetic depths among flowering plant families and genera of  
96 species spanning three diverse clades within the order Malpighiales (Malpighiaceae,  
97 Chrysobalanaceae, and Elatinaceae). Finally, we demonstrate the generality and scalability  
98 of varKoding across the Tree of Life by testing it on several published species-level datasets  
99 from fungi, plants, animals, bacteria, and finally from a massive dataset including all  
100 families of eukaryotes from publicly available sequence data.



101

102 **Figure 1.** varKoding and training data overview. (A) varKode generation workflow. varKode images are  
 103 natively grayscale, but here they are mapped to a rainbow color scale for increased contrast. (B) Phylogeny  
 104 and example varKodes of *Stigmaphyllon* species. (C) Phylogeny and example varKodes of Malpighiaceae  
 105 genera including their closest outgroup (*Elatine*, Elatinaceae). (D) Examples of varKodes from across plant  
 106 families of Malpighiales, and (E) across kingdoms. Chronograms depicted for each representative set with  
 107 timelines in millions of years (Myr) at the bottom of B and C.

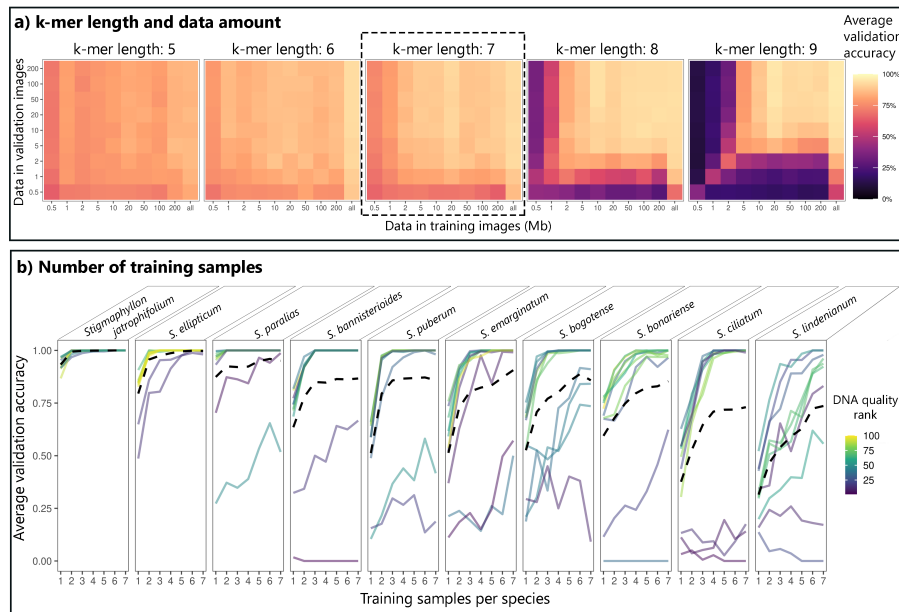
# 108 Results and Discussion

## 109 varKodes can be classified with neural networks

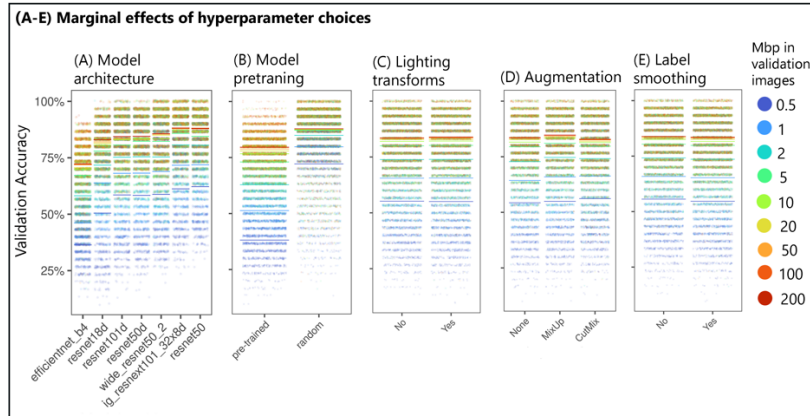
110 An accurate and scalable DNA-barcoding method using neural networks has not previously  
111 been developed owing to two widely held misconceptions: i.) accurate barcoding by neural  
112 networks requires sufficiently large training data sets that they would be impractical for  
113 typical applications<sup>59</sup>; and ii.) existing neural network architectures for image classification  
114 are inadequate for species barcoding<sup>42</sup>. In contrast, our analysis demonstrates that  
115 carefully designed varKodes analyzed with existing neural network architectures  
116 optimized for image classification can identify taxa with very high accuracy even from  
117 modest amounts of data. varKodes use short k-mer counts from raw sequencing reads to  
118 create a snapshot of the total genomic landscape for a given sample. Variation in varKodes  
119 can be small but remain visually perceptible among species (e.g., of *Stigmaphyllon*, **Figure**  
120 **1B**) and genera (e.g., of Malpighiaceae, **Figure 1C**). Variation is more striking among higher  
121 levels of phylogenetic divergence, such as between families in the order Malpighiales  
122 (**Figure 1D**) or different kingdoms of eukaryotes and prokaryotes (**Figure 1E**). We  
123 expected, therefore, that neural network architectures developed for image classification,  
124 (e.g., resnets<sup>60</sup> or vision transformers<sup>61</sup>) would be able to differentiate varKodes.

125  
126 We first optimized hyperparameters and training conditions to maximize accuracy for  
127 species-level identification of *Stigmaphyllon*. We identified that varkodes depicting k-mer  
128 length = 7 struck a good balance between accuracy and the amount of input sequence data  
129 (**Figure 2A**). Furthermore, models trained with augmented data from several subsampled  
130 images drawn from each individual exhibited substantially better performance and greater  
131 robustness (**Figure 2A**). A linear model demonstrated that neural network architectures  
132 and training methods designed for image classification of photographs<sup>60, 62, 63, 64, 65</sup> are  
133 extremely useful for varKode-based identification, contrary to suggestions that  
134 classification of similar images requires specialized architectures<sup>42</sup>. Specifically, we  
135 observed increased accuracy with more parameter-rich neural network architectures  
136 (*ResNeXt101*<sup>66</sup>, among those tested), augmentation with lighting transformations, *CutMix*<sup>65</sup>

137 and *MixUp*<sup>64</sup>. Label smoothing<sup>67</sup> and pretraining models on photographs decreased  
 138 accuracy (**Figure 3**). We also identified that these approaches enabled training with very  
 139 modest datasets: four samples per taxon was sufficient for 100% median accuracy (**Figure**  
 140 **2B**). Errors in species identification were concentrated among sequences derived from  
 141 herbarium samples that demonstrated evidence of DNA damage as is sometimes reported  
 142 for ancient DNA<sup>68</sup> (**Figure 2B**). However, we identified that the inclusion of low-quality  
 143 training samples decreased validation accuracy only among other low-quality samples but  
 144 not among high-quality ones (**Figure 4**).

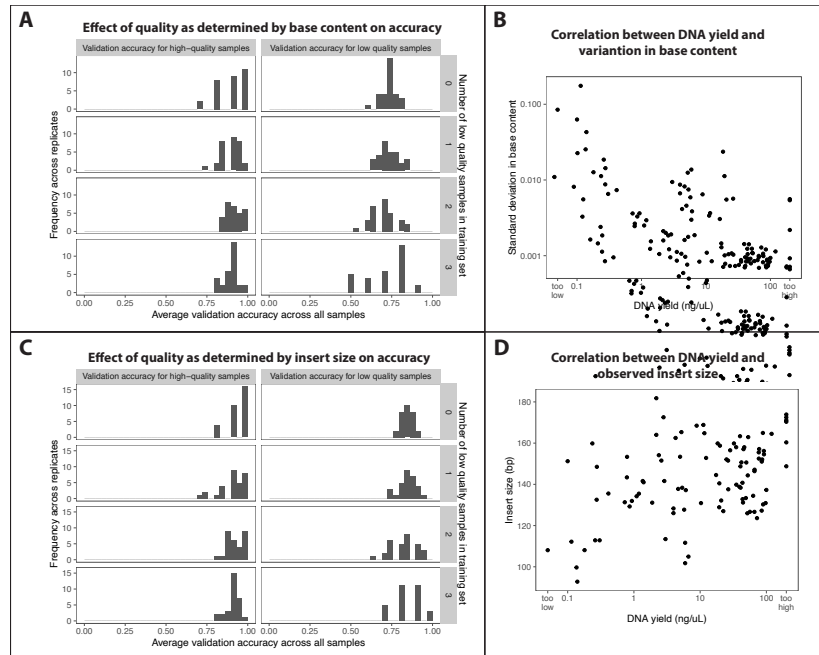


145  
 146 **Figure 2. Neural network training of varKodes for species identification. (A)** Effect of k-mer length and  
 147 data amount used to produce varKodes on validation accuracy. Longer k-mers increase accuracy when more  
 148 data are used. Mixing varKodes subsampled from different amounts of data improves accuracy. Box with  
 149 dashed line (k-mer length = 7) strikes a good balance between model accuracy and amount of required data.  
 150 **(B)** Validation accuracy improves with increased number of training samples per species, but even 3–4  
 151 samples are sufficient in most cases for achieving high accuracy. Each solid line represents one sample,  
 152 colored by DNA quality (i.e., variation in base pair frequencies). Higher rank indicates better quality. Dashed  
 153 lines represent averages across all samples.



154  
 155 **Figure 3.** Marginal effects of neural network model and training options. Dots represent individual replicates,  
 156 and bars depict averages. All parameters were identified to be significant in a linear model: more complex  
 157 model architectures, lighting transformations, and augmentation methods *MixUp* and *CutMix* improved  
 158 accuracy. However, pretraining with large image datasets and label smoothing decreased accuracy.

159  
 160 We hypothesized that lower-quality samples shared similar sequences resulting from  
 161 common patterns of DNA damage and greater levels of microbial or human contaminants,  
 162 resulting in spurious similarities in varKodes (**Figure 5**). Contaminants are thought to  
 163 increase errors in genome skim methods<sup>69</sup>. To mitigate this problem, we applied multi-  
 164 label classification<sup>70</sup> to our neural network models. While single-label classification models  
 165 always return a single prediction (that is, an inferred label), multi-label models can return  
 166 zero or more predictions, resulting in higher robustness to spurious patterns of similarity.  
 167 For a set of samples with known labels used for validation, a prediction is a true positive if  
 168 the predicted label matches the actual label, and a false positive if not. Failure to predict an  
 169 actual label is deemed a false negative. For each validation sample, we summarized  
 170 predictions as i.) correct (true positives only), ii.) incorrect (false positives only), iii.)  
 171 ambiguous (multiple predictions, including true and false positives), or iv.) inconclusive  
 172 (no prediction). For each test, we summarized results across all validation samples using  
 173 two metrics: precision (the sum of all true positives divided by the sum of all true and false  
 174 positives) and recall (the sum of all true positives divided by the sum of all true positives  
 175 and negatives).



176

177

178

179

180

181

182

183

184

185

186

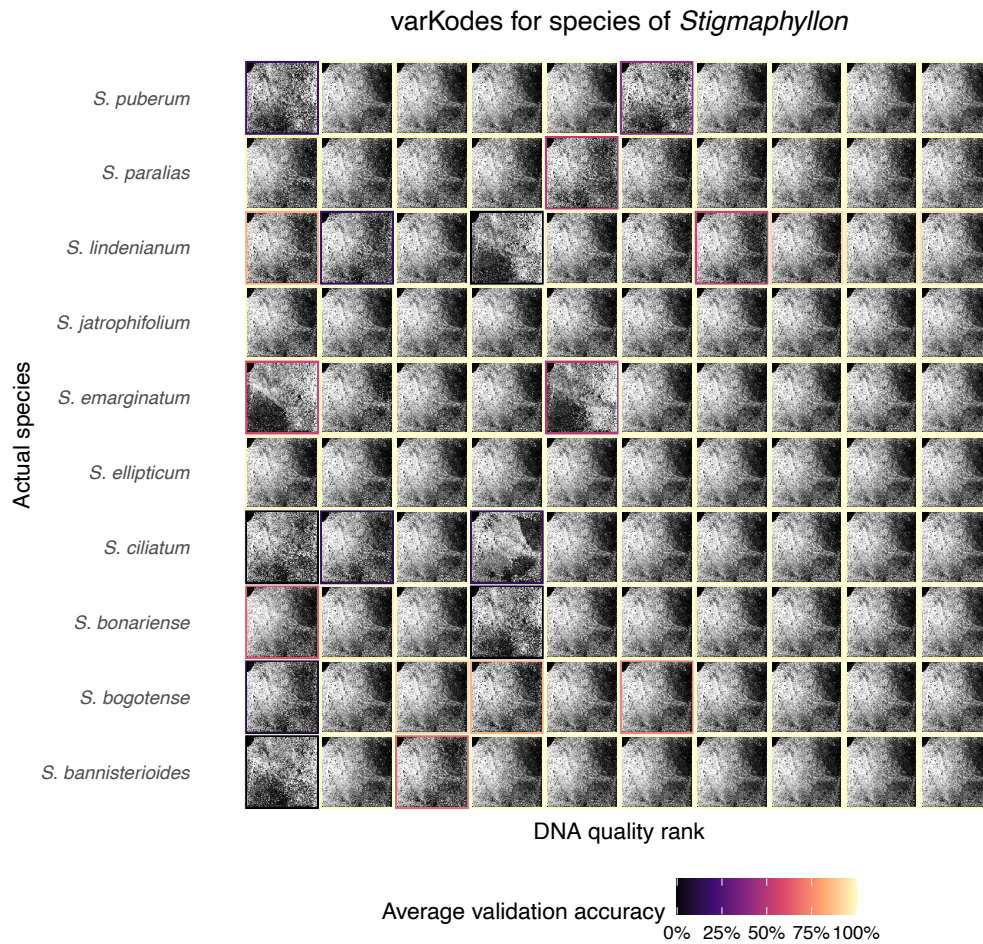
187

188

189

**Figure 4.** Effect of the inclusion of low-quality training samples, inferred from variation in base pair content (A, C) or insert size (B, D). Increasing the fraction of samples in the training set that were low-quality did not strongly affect the average validation accuracy, but it increased dispersion. Low-quality samples are the four samples with highest variation in base-pair content or shortest insert size in raw reads for each species. Panels **B** and **D** show the correlation of each quality metric with DNA extraction yield.

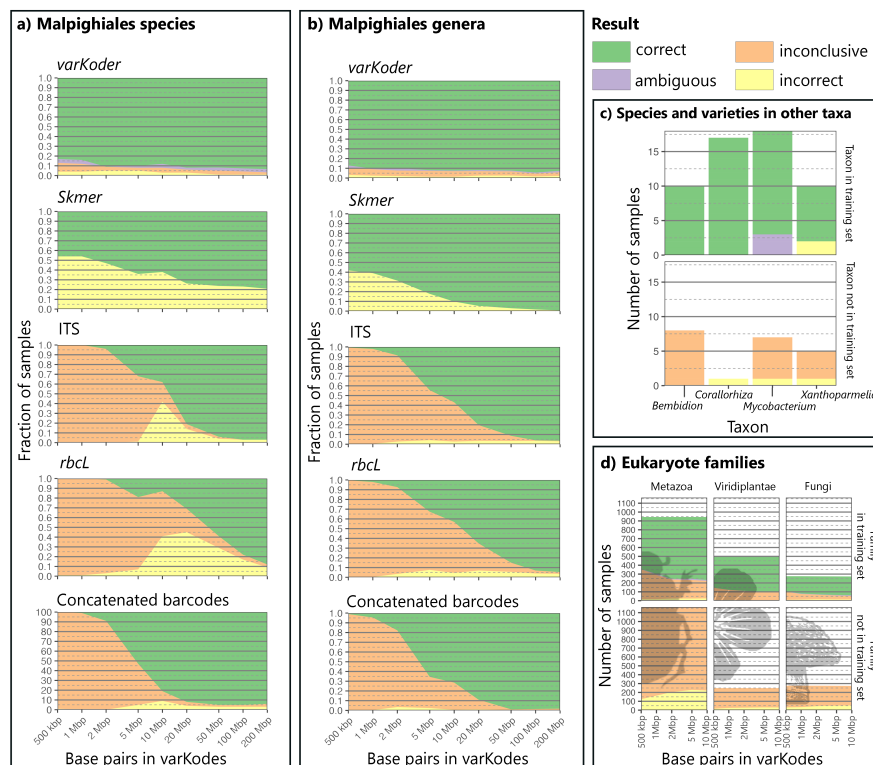
In summary, we developed and tested a robust and scalable method of DNA barcoding capable of training with small amounts of data, and implemented it in the *varKoder* software, which can process sequence data required to generate varKodes, train an image-classification neural network using varKodes, and query new data with a trained neural network. These tasks are accomplished with widely used tools for sequence processing<sup>71, 72, 73, 74, 75</sup> and for neural network training<sup>76, 77, 78</sup>.



190  
191  
192  
193  
194  
195  
196  
197  
198  
199  
200  
201  
202

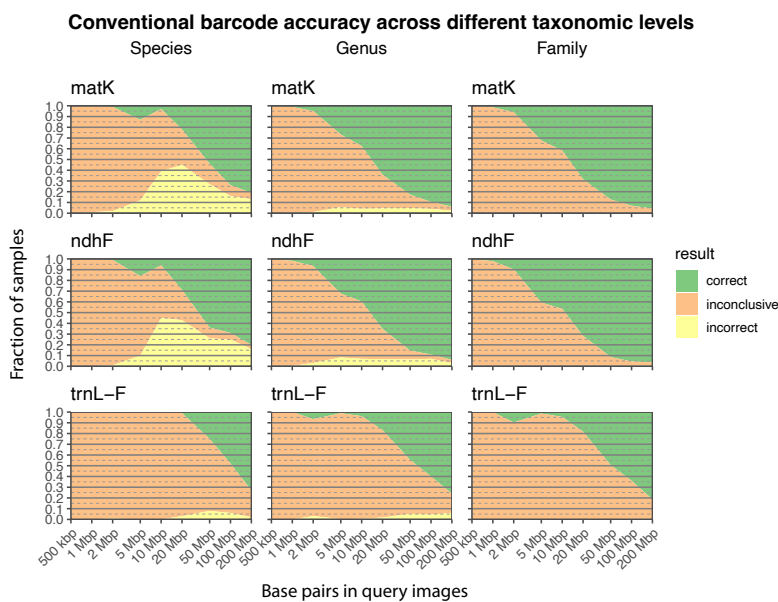
**Figure 5.** Low-quality DNA may lead to spurious patterns of similarity in varKodes. Samples with lower quality show varKode patterns divergent from their species more often than high-quality ones. These divergent patterns may be similar between low-quality samples across species. These samples also show reduced validation accuracy in a single-label model. For each sample, we show the varKodes produced from all DNA data available. Within each species, samples are organized from lowest (left) to highest (right) DNA quality. Bounding boxes around each sample indicate the average validation accuracy across 30 random replicates with 7 training samples per species.

203 **varKodes are highly accurate for identification of species, genera, and families.**  
 204 To test varKodes under a real-world scenario with heterogeneous data (e.g., large numbers  
 205 of taxa, multiple replicates per taxon, varying sequence depth and sample quality), our *de*  
 206 *novo* assembled genomic data set included 287 accessions: 100 samples of *Stigmaphyllon*  
 207 from our initial development outlined above, plus additional genera in the families  
 208 Malpighiaceae (30 genera; 151 samples), Chrysobalanaceae (8 genera; 30 samples), and  
 209 Elatinaceae (1 genus; 6 samples) in the order Malpighiales. Using these data, we first  
 210 demonstrated high cross-validation accuracies for species identity of *Stigmaphyllon* (83.0–  
 211 93.4% correct, 91.5%–95.7% precision, 87%–96.7% recall depending on data input  
 212 amount; **Figure 6A**). Most errors were inconclusive or ambiguous predictions, and not  
 213 incorrect assignments.



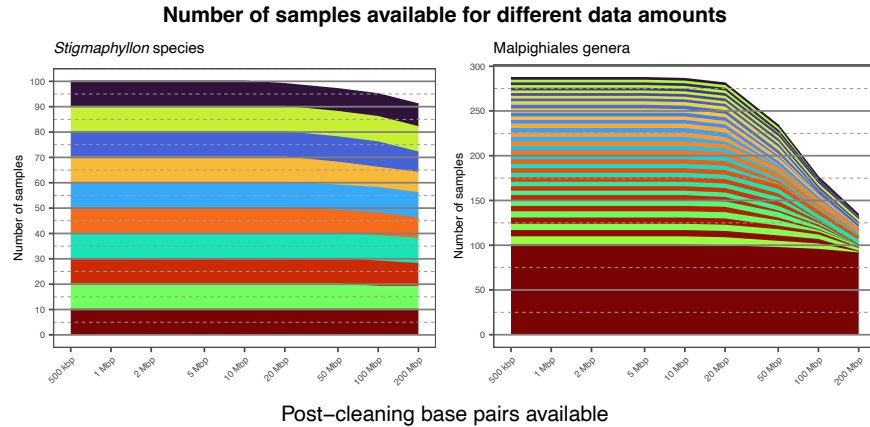
214  
 215 **Figure 6.** Performance of *varKoder* and alternative barcoding methodologies across different data sets. (A)  
 216 Leave-one-out cross-validation to identify species of Malpighiales using different approaches and amounts of  
 217 data to assemble query samples. (B) Same as (A), but for genera. (C) Performance for species-level  
 218 identification across different publicly-available datasets: *Bembidion* beetles, *Corallorhiza* orchids,  
 219 *Mycobacterium tuberculosis* bacteria, and *Xanthoparmelia* fungi. All query samples used as much data as were  
 220 available. (D) Performance for Eukaryote family-level identification for different amounts of input data.

221 *varKoder* is also robust to the amount of input sequence data necessary for model training,  
 222 performing well even at the lower range of input data (**Figure 6A**). Assuming an average  
 223 genome size of about 2 Gbp for Malpighiaceae<sup>79</sup>, the very small amount of genome skin  
 224 data used to generate varKodes represented coverages of less than  $\sim 0.0002\times-0.107\times$ .  
 225 Moreover, when compared to cross-validation accuracies of existing alternatives, *varKoder*  
 226 accuracy is higher than *Skmer*, which showed 46% correct predictions (57.5% precision,  
 227 46% recall) with minimal data amounts and peaked at 79.1% for the larger data amounts  
 228 (80% precision, 79.1% recall, **Figure 6A**). On the other hand, traditional barcodes  
 229 including individual plastid genes and nuclear ribosomal ITS regions performed well for  
 230 both BLAST-based (25–97% correct, 66.6–97.3% precision, 25–97% recall depending on  
 231 the gene) and phylogenetic-based (94–95% correct, >99% precision, 97.2–98.4% recall for  
 232 concatenated matrices) approaches when at least 50 Mbp of data was provided (**Figure 6A**,  
 233 **Figure 7**). However, these results were much worse when <50 Mbp of data were available  
 234 (down to zero correct for BLAST), with unsuccessful locus assembly leading to inconclusive  
 235 predictions as the primary reason for the failure (**Figure 6A**, **Figure 7**). In summary,  
 236 *varKoder* reaches much higher accuracy for species determination than existing methods  
 237 for unprecedentedly small amounts of data and demonstrates similar accuracies for  
 238 datasets when greater amounts of sequence data are available.



239  
 240 **Figure 7.** Accuracy of conventional barcode loci for species, genera and families within the Malpighiales.

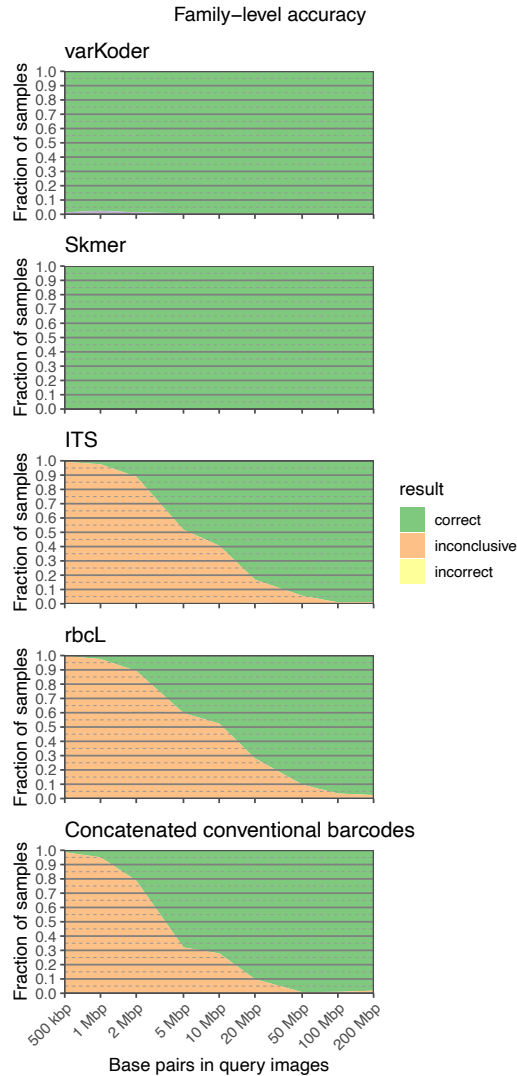
241 Genus-level identification yielded similar high accuracies with *varKoder* (87.1–94.3%  
242 correct, 94.1%–97.4% precision, 89.1%–95.4% recall depending on input amount, **Figure**  
243 **6B**), but with a higher rate of inconclusive predictions (2.8–7.6%). A linear model  
244 demonstrated that this higher uncertainty can be attributed to two factors: i.) samples  
245 exhibiting higher levels of DNA damage in genera other than *Stigmaphyllon* and ii.) genera  
246 trained with fewer replicates (e.g., down to 3 samples for some genera; **Figure 8**).  
247 Additionally, samples within genera share fewer genetic similarities than samples within  
248 species, which likely poses a more challenging classification problem. However, the  
249 incorrect rate is very small in all cases (1.4–3.1%) with most errors being inconclusive or  
250 ambiguous predictions. In contrast, *Skmer* exhibited better performance when larger  
251 amounts of data were used (99.2% correct, 99.2% precision, 99.2% recall for 200 Mbp),  
252 but performed poorly for lower amounts of data like those commonly generated from  
253 genome skim experiments (58.2% correct, 58.2% precision, 58.2% recall for 500 Kbp)  
254 (**Figure 6B**). Genus-level identifications using conventional barcodes in a concatenated  
255 phylogeny were up to 98.1% correct (99.2% precision, 97.2% recall) when a large amount  
256 of data (200 Mbp) was available (**Figure 6B**). But like its application at species-level  
257 identification, most predictions were inconclusive when less than 20 Mbp reads were used  
258 (**Figure 6B**). Although genome skimming can be used to sequence conventional barcodes,  
259 they are more often obtained with amplicon sequencing, which has failure rates ranging  
260 from 15–75% even with highly optimized protocols<sup>80</sup>. Therefore, conventional barcodes  
261 have a high number of inconclusive predictions also with amplicon sequencing. At the  
262 family level, *Skmer* and *varKoder* had near-perfect accuracy across all data amounts (>97%  
263 correct), while conventional varKodes performed well when there was sufficiently large  
264 amounts of data (**Figures 7, 9**). We note that 135 of our 287 *de novo* assembled genome  
265 skim samples had at least 200Mbp of available data (**Figure 8**), and these are enriched for  
266 specimens that performed well in DNA library preparation and sequencing. As a result, the  
267 good performance across methods for the highest data amounts may result partly from  
268 higher-quality DNA yielding more reads with more even genome coverage.



269  
 270 **Figure 8.** Number of samples available for different data amounts in each dataset. Arbitrary colors are  
 271 assigned to individual taxa.

272  
 273 **varKodes are universal and scalable across the Tree of Life.**

274 To further test the universality of varKodes, we expanded the testing of our tool using  
 275 published data from diverse clades of plants, fungi, animals, and bacteria (**Figure 6C**).  
 276 These tests included species-level identification in insects (*Bembidion* beetles<sup>81, 82</sup>) and  
 277 lichen-forming fungi (*Xanthoparmelia*<sup>83</sup>), species and infra-specific taxon identification in  
 278 coralroot orchids (*Corallorhiza*<sup>84</sup>), and clinical isolate identification of evolved strains of  
 279 human pathogenic bacteria (*Mycobacterium tuberculosis*<sup>85</sup>). In all cases, we tested the  
 280 performance of *varKoder* on taxa included in the training set and on taxa not included in  
 281 the training set. We identified perfect species identification (100% correct, 100% precision,  
 282 100% recall) for beetles and coralroot orchids included in the training set. For bacteria,  
 283 16% of the validation set returned ambiguous assignments; the remaining samples were  
 284 correctly identified (85.7% precision, 100% recall). In lichen-forming fungi, which include  
 285 DNA from both the fungal and algal partners, and thus are more challenging, 20% of the  
 286 test samples returned incorrect assignments; the remainder were correct (80% precision,  
 287 80% recall). For all cases, species or varieties not included in the training set generally  
 288 resulted in inconclusive results, with a minority yielding incorrect predictions (**Figure 6C**).



289  
 290 **Figure 9.** Comparison of *varKoder*, *Skmer*, and conventional barcode accuracy for identifying families of  
 291 Malpighiales.

292  
 293 Finally, we tested the universality and scalability of varKodes by training a single model to  
 294 identify all 861 eukaryotic families from at least three accessions per family compiled from  
 295 the NCBI Sequence Read Archive. Owing to NCBI download bottlenecks, we restricted  
 296 varKode construction to a more restricted amount of data per sample, downloading up to  
 297 only 10 Mbp of data. This exercise achieved a rate of correct predictions of 62.1–79.6%  
 298 across all kingdoms when families were included in the training set (**Figure 6D**), with most  
 299 errors being inconclusive predictions (14.2–33.3%). Precision varied from 95% to 97%  
 300 and recall from 65% to 78%. Similarly to the species- and variety-level exercise, families

301 not included in the training set often yielded inconclusive predictions **(Figure 6D)**,  
302 suggesting a potential for varKoding to be used as a discovery tool when reasonably well-  
303 sampled training data sets are available.

304  
305 As we note above, a single model classifying all eukaryotic families is not possible with  
306 conventional barcodes, since they are not universal. This is a central limitation of  
307 conventional barcodes. *Skmer*, the state-of-the-art genome skimming alternative, cannot be  
308 scaled to a dataset of this size: our attempt to apply it could not be finished after more than  
309 40 days using 32 high-performance computing cores. In general, conventional barcodes,  
310 when derived from genome skimming data, require memory- and processor-intensive  
311 sequence assembly, and *Skmer* relies on pairwise all-by-all sample comparisons; its  
312 computing time and required storage both increase quadratically with the number of  
313 samples. Neural network models, on the other hand, have a fixed size, independent of the  
314 number of samples used in training, and training time scales linearly with the number of  
315 input samples. Our most complex model, trained with all eukaryote families, has about  
316 1.3GB of disk size. varKodes images also are tiny (8.2 KB on average for k-mer length of 7)  
317 replacements to much larger genomic data sets (on average, 144 MB per sample here). A  
318 varKode model potentially trained on millions of species can therefore easily be ported to  
319 devices without continuous internet access, thus allowing for more widely distributed  
320 applications of varKoding, such as field-laboratory environments or proposed distributed  
321 genetic databases<sup>86</sup>. Hence, varKodes are not only comparable across the entire Tree of Life  
322 but also can leverage existing and widely available computer hardware to provide accurate  
323 and fast identifications commensurate to the scale of Earth's biodiversity.

324

## 325 **Conclusions**

326 varKoding represents a major advance in inventorying Earth's biodiversity. They are  
327 universal, accurate, efficient, and hold tremendous promise for scalability and adaptability.  
328 varKodes are applicable to organisms with simple or complex genomes. Although our focal  
329 test clade from Malpighiaceae specifically is known to exhibit high variation in ploidy  
330 across the family<sup>87, 88</sup>, it did not interfere with our efforts. Indeed, further exploration may

331 reveal that these sorts of macrostructural genomic properties form the basis of key  
332 varKode differences between some clades. In particular, varKodes i.) provide accurate  
333 identification with far less data than existing methods that use next-generation sequence  
334 data; ii.) are universal across the Tree of Life; iii.) demonstrate enhanced computational  
335 efficiency and scalability; and iv.) are modular and can improve with time alongside  
336 innovations in sequencing technologies, bioinformatics, and machine learning. Reference  
337 data for varKoding will be increasingly available from ambitious efforts including the Earth  
338 Biogenome Project<sup>89</sup>, the African Biogenome Project<sup>90</sup>, the 10,000 Plants Genome Project<sup>91</sup>,  
339 and the Vertebrates Genome Project<sup>92</sup>. We also note that varKoding is much easier and  
340 cost-effective to obtain from low-coverage genome skims than high-quality contiguous  
341 genomes. For example, our cost for a 3× skim of herbarium samples is about \$34 per  
342 sample, versus a high-quality genome which may cost tens-of-thousands of dollars each.  
343 Although varKodes inevitably will benefit from the aforementioned large-scale sequencing  
344 initiatives, a concerted effort to obtain genome skims from museum type specimens and  
345 other representative specimens could have a larger impact in a far shorter amount of time  
346 than sequencing high-quality genomes. For example, the majority of our Malpighiales  
347 samples were derived from herbarium specimens, some more than 110 years old and  
348 presently less suitable for chromosomal-level genome assembly. Thus, varKodes show  
349 tremendous promise for further automating species identification from herbaria and other  
350 natural history collections<sup>93</sup>. Such multiomic efforts represent a new frontier of  
351 biodiversity discovery but should be advanced effectively and ethically to preserve and  
352 protect the biodiversity heritage represented in global natural history collections for future  
353 use<sup>94, 95</sup>.

354

355 We expect that varKoding will be invaluable to the biodiversity science community in  
356 numerous ways. One avenue to be explored is its utility for the identification of samples  
357 with poor-quality and degraded DNA, such as unidentified fragmentary fossil and subfossil  
358 remains in natural history collections<sup>96, 97</sup>. Because our method relies on counts of very  
359 short k-mers (7 bp), they are well-suited for varKodes while other barcoding methods are  
360 not possible. Moreover, we explicitly labeled and classified samples based on their

361 taxonomic identities, but varKodes could in principle be used to classify a set of sequences  
362 based on any kind of metadata, as long as sufficient training data are available. For  
363 example, varKodes likely will be useful for environmental sampling initiatives in which the  
364 entire genomic composition of a sample spanning multiple species can be characterized  
365 (varKoded), even if *varKoder* is not optimized to recognize individual species or genes  
366 within a mixed sample. For example, we envisage that varKodes could be useful to  
367 correlate aquatic eDNA samples to location and water quality, to ascertain the origin of a  
368 sample for forensic study, or to help trace the geographic origin of organisms seized  
369 during transit suspected of illegal harvesting.

## 370 **Methods**

### 371 **Data**

372 *Taxon sampling, DNA sequencing, assembly, and annotation for newly acquired genetic*  
373 *data*—Our newly generated plant data set included three flowering plant families, all  
374 members of the large and diverse order Malpighiales<sup>34</sup>: Malpigiaceae, Elatinaceae, and  
375 Chrysobalanaceae. The Malpigiaceae data are the most taxonomically comprehensive and  
376 include 251 accessions representing 161 species, which were sampled from 248 herbarium  
377 specimens and three silica-dried field collections. These represent 30 genera. Among these  
378 data, *Stigmaphyllon* has the most comprehensive species sampling, including 10 species  
379 and 10 accessions sampled per species. Elatinaceae includes 6 samples from 6 different  
380 species in the genus *Elatine*, and Chrysobalanaceae includes 30 accessions representing 30  
381 species in 8 genera. All 100 *Stigmaphyllon* samples were sequenced specifically to build,  
382 validate, and test our identification models at shallower phylogenetic depths and were  
383 consequently labeled with species, genus, and family names. A key advantage of sampling  
384 *Stigmaphyllon* is that its taxonomy has been extensively revised by coauthor C. Anderson<sup>57</sup>,  
385 <sup>58</sup>. Plants exhibit notoriously complex genomic architectures<sup>98</sup>, rendering them a good test  
386 case for our investigation. Moreover, the *Stigmaphyllon* clade represents a wide array of  
387 divergence times that span distantly- (30.8 millions of years, Myr) to very closely-related  
388 (0.6 Myr) species (**Figure 1**). The focus for the remainder of the Malpigiaceae,

389 Chrysobalanaceae, and Elatinaceae sampling was to identify a given sample to genus. In  
390 this case, among the non-*Stigmaphyllon* samples we included 3–9 species per genus  
391 representing 29 genera of Malpighiaceae, eight of Chrysobalanaceae, and one of  
392 Elatinaceae. Each generic representative was labeled with its corresponding genus and  
393 family identification. Unlike *Stigmaphyllon*, where we included multiple accessions per  
394 species, there were no additional replicates per species for our genus-level sampling.  
395 We used total genomic DNA extractions detailed previously for our newly included  
396 Malpighiales data<sup>54, 99</sup>. Where applicable, we isolated total genomic DNA from 0.01–0.02 g  
397 of silica-dried leaf material or, more commonly, herbarium collections using the Maxwell®  
398 16 Tissue DNA Purification Kit (Promega Corporation, Inc., Madison, WI, USA). Genomic  
399 libraries were prepared using ca. 70 ng of genomic DNA per sample where possible. For  
400 DNA library preparation we used the Kapa HyperPlus library prep (Kapa Biosystems, Inc.,  
401 MA, USA) with Nextflex-Ht barcodes (Bioo Scientific Corporation, TX, USA) and IDT  
402 TrueSeq barcodes (Integrated DNA Technologies, Inc., IO, USA), fragmenting DNA to 350–  
403 400 base pairs (bp), and indexing for Illumina multiplex sequencing. We verified the DNA  
404 concentration of these libraries, and fragment sizes using the Qubit dsDNA HS Assay Kit on  
405 a Qubit 2.0 Fluorometer (Invitrogen, Carlsbad, CA, USA), and the Agilent TapeStation 2200  
406 (Agilent Technologies, Inc., Waldbronn, Germany). All total genomic DNA libraries were  
407 diluted to 0.7 nM, pooled, and sequenced with the Illumina Hi-Seq 2x125 on the Genome  
408 Analyzer II (Illumina, Inc., San Diego, CA, USA) at the Bauer Core Genomics Sequencing Core  
409 Facility at Harvard University, MA, USA. The genome skimming pipeline we applied is  
410 described by Weitemier *et al.*<sup>100</sup> and has been extensively applied in studies by members of  
411 our coauthor group<sup>101, 102, 103</sup>.

412

413 *Public genomic data compilation*—To further understand the versatility of *varKodes* more  
414 broadly across the Tree of Life, we tested species identification using genome skim data  
415 sets from four genera of plants, animals, fungi, and a bacterial species. This involved a plant  
416 data set from coralroot orchids (genus *Corallorhiza*), a well-delineated clade of  
417 mycoheterotrophic orchids<sup>84</sup>. This data set allowed us to assess the utility of *varKodes* for  
418 identifying infraspecific taxa: *Corallorhiza striata* includes several well-known and easily

419 identifiable varieties. For animals, we assembled a *Bembidion* beetle data set, which  
420 includes well-known closely related cryptic species<sup>81, 82</sup>. For fungi, we used  
421 *Xanthoparmelia*, a lichen-forming genus with fungal symbionts whose species are poorly  
422 understood and which often form paraphyletic species groupings<sup>83</sup>. Finally, our bacterial  
423 data set was from *Mycobacterium tuberculosis*, the species of pathogenic bacteria that  
424 causes tuberculosis. This genomic data set consisted of clinical isolates from five distinct,  
425 monophyletic lineages of *M. tuberculosis* and enabled us to understand how varKodes  
426 function on an extremely recently diverged, clinically relevant bacterial lineage<sup>85</sup>. This data  
427 set of clinical isolates from human-adapted lineages exhibited 99.9% sequence similarity  
428 despite key differences in phenotypes, including drug resistance, virulence, and  
429 transmissibility<sup>85</sup>. *Mycobacterium tuberculosis* has diversified quite rapidly in humans, with  
430 nine monophyletic lineages. Divergence time estimates for the most recent common  
431 ancestor of *M. tuberculosis* are <6,000 years ago<sup>104</sup>.

432 In all the above cases, we included taxa with at least two samples in the training set when  
433 using publicly available data. Our validation set consisted of randomly selected samples  
434 from these taxa. We additionally validated the model on samples from taxa with only one  
435 sample available, and, therefore, not included in the training set. Each of these four data  
436 sets were downloaded using the NCBI Sequence Read Archive.

437 In addition to these species-level datasets, we used NCBI Entrez to query all of the data  
438 available on SRA for Eukaryotes. We then filtered this list to accessions generated with  
439 Illumina technology and containing at least 50 million base pairs. From this filtered list, we  
440 selected all families with at least three subtaxa containing sequences. We then randomly  
441 selected one accession per subfamilial taxon, and up to 20 subtaxa per family. We used  
442 fastq-dump (<https://trace.ncbi.nlm.nih.gov/Traces/sra/sra.cgi?view=software>) to  
443 download up to 500,000 spots for each accession and used these to generate varKodes  
444 from 500kbp to 10Mbp of data. In each family, 80% of the accessions were used in training  
445 and the remaining 20% were used for validation. To validate model behavior for taxa not  
446 included in the training set, we downloaded all accessions from SRA in families of plants,  
447 animals, and fungi excluded from the training set but containing at least one sample with at  
448 least 50 million base pairs of data.



450 **Initial varKode design and testing**

451 *varKode sequence data preprocessing*—We designed images—**varKodes**—that portray  
452 relative frequencies of k-mers from low-coverage raw Illumina reads. These are similar to a  
453 ‘chaos game representation’ *sensu* Jeffrey<sup>53</sup>, but optimized for raw reads in which sequence  
454 orientation is unknown (and therefore k-mers and their reverse complement are  
455 indistinguishable). We call these varKodes because they enCODE the VARIation in k-mer  
456 frequencies in a sample.

457 To avoid sequencing artifacts, raw Illumina reads were lightly cleaned prior to k-mer  
458 counting and involved the following steps: identical reads were de-duplicated using  
459 *clumpify.sh* as implemented in BBtools<sup>72, 105</sup>, adapters were removed, low-quality tails  
460 trimmed, and overlapping read pairs merged using *fastp*<sup>74</sup>. Next, we randomly selected  
461 subsets of cleaned reads with predefined data amounts, ranging from 500 kbp to 200 Mbp.  
462 These data subsets were used to generate a variety of input varKodes for a single sample  
463 and all such images were used for training (see main text and Figure 2A). Finally, we  
464 applied *dsk*<sup>73</sup> to count k-mers of a given length based on clean raw reads. *dsk* exhibits good  
465 performance with low memory requirements, which is ideal for potential applications  
466 using varKodes on low-memory devices. We note that analyses for species-level public  
467 datasets have low compute requirements and were performed on an Apple MacBook with  
468 ARM processor architecture. Bioinformatics and image classification application of this  
469 nature are typically thought to be possible only in more resourced computer servers<sup>41</sup>, but  
470 our method demonstrates that this is not the case.

471  
472 *k-mer to image mapping*—We developed a two-dimensional mapping of k-mers to pixels to  
473 create the varKode image. Each unique k-mer has a unique pixel location on the varKode. A  
474 desirable property of this mapping is that more similar k-mers exhibit greater spatial  
475 adjacency. We first began by listing all possible canonical k-mers to generate the mappings  
476 for k-mer lengths between 5 to 9. To identify which k-mers were more similar to each  
477 other, we counted, for each k-mer, the occurrence of smaller sub k-mers and then grouped  
478 them based on greater or lesser overall similarity. For example, each possible 5-base-pair  
479 sequence can be represented uniquely by the counts of subsequences of lengths 2 and 3

480 contained within it and compared similarly across other k-mers. Likewise, each possible 9-  
481 base-pair sequence can be represented uniquely by the counts of subsequences of lengths  
482 2, 3, and 5. Moreover, since our method works with raw reads, the orientation of each  
483 sequence is unknown and therefore each k-mer represents itself and its reverse  
484 complement. For this reason, we averaged counts for each canonical k-mer and its reverse  
485 complement.

486 Next, we applied *t-SNE*<sup>106</sup>, a non-linear dimensionality reduction method, to group k-mers  
487 based on their relative similarity. This allowed us to reduce canonical k-mer representation  
488 into a two-dimensional space. We noticed from this output that *t-SNE* separated k-mers  
489 mainly by AT richness, so we rotated coordinates to make this the main left-to-right axis.  
490 Next, we transformed these data mapped in continuous space to pixels in a square grid  
491 forming the initial varKode. Our square grid was constructed with the minimum size  
492 required to fit each individual canonical k-mer to a unique grid cell (pixel). After rescaling  
493 continuous *t-SNE* coordinates, we assigned each k-mer to the closest available pixel, using  
494 randomization in the cases in which more than one k-mer overlapped in a single pixel. This  
495 procedure resulted in a mapping that uniquely assigns each k-mer to a pixel in the varKode.  
496 Once we established the two-dimensional mapping of each k-mer to the varKode, we  
497 developed a method for transcribing k-mer counts to be represented as pixel brightness. To  
498 make varKodes as compact as possible, we used 8-bit grayscale images. As a result, for a  
499 typical 8-bit grayscale image format, we have 256 possible brightness levels per pixel.  
500 Therefore, raw k-mer counts had to be mapped to 256 values while maintaining relevant  
501 information on their variation. Because k-mer counts vary across many orders of  
502 magnitude, we first rank k-mers based on their absolute counts. We attempted alternative  
503 data transformations with the same goal in our early iterations, including log and square-  
504 root, but these were less successful in terms of final model accuracy. The ranks were  
505 subsequently sorted into 256 bins, and these represent the values used to translate ranks  
506 to pixel brightness to finalize each varKode. The varKode image is saved as a compressed  
507 png file. These operations use python libraries *numpy*<sup>76</sup> and *pillow*<sup>107</sup>.

508

509 *Testing the effect of k-mer length and data amount*—We chose neural network models to  
510 compare varKodes because of their enhanced ability to handle images and identify complex  
511 patterns within them. We employed *fastai*<sup>78</sup> for this purpose, a high-level implementation  
512 of neural networks based on *pytorch*<sup>77</sup>. All of the model architectures we applied are image  
513 classification models available from the *timm* library<sup>108</sup>, which have been widely tested  
514 using a variety of image types. To identify the optimal training hyperparameters for our  
515 neural network, we conducted a series of tests using our species-level data set for the  
516 genus *Stigmaphyllon*. We generated varKodes for each of the *Stigmaphyllon* samples using  
517 the workflow described above. We first tested the joint effect of k-mer length and input  
518 data amount for neural network classification accuracy by selecting three samples per  
519 species as a validation set; the remaining samples were used to train neural networks using  
520 different amounts of input data across 10 randomly generated training sets. As input data  
521 for both the validation and training sets, we randomly subsampled the original sequences  
522 into fastq files containing from 500 Kb to 200 Mb (equivalent to about 1,700 to 670,000  
523 2x150bp Illumina reads). In this test, we only included samples that yielded at least 200  
524 million base pairs after cleaning. We also tested the effect of combining images for all data  
525 amounts in training. For each replicate, we applied the widely used image classification  
526 neural network *resnet50* architecture<sup>109</sup> to classify varKodes and trained models for 30  
527 epochs. We visualized the distribution of validation accuracy for each combination of input  
528 data amount and k-mer lengths to find a good balance between both.

529  
530 *Neural network optimization*—After identifying an appropriate k-mer length and input data  
531 used to produce varKodes, we next tested a series of neural network training conditions.  
532 We varied the neural network model complexity, choosing from seven commonly used  
533 architectures: *resnet50*<sup>109</sup>, *resnet-D*<sup>60</sup> with different depths (18, 50, 101), a wide *resnet50*<sup>60</sup>,  
534 *efficientnet-B4*<sup>110</sup>, and *ResNeXt101*<sup>66</sup>. We also tested the effect of the following: random  
535 initial weights vs pretrained weights from the *timm* library<sup>108</sup>, presence or absence of  
536 lighting transforms, presence or absence of label smoothing, and presence or absence of  
537 augmentation strategies (i.e., *CutMix*<sup>65</sup> or *MixUp*<sup>64</sup>). Because these parameters may have  
538 complex interactions, we tested all combinations of architecture, pretraining, transforms,

539 label smoothing, and augmentation, with 20 replicates for each combination of conditions.  
540 In each replicate, we randomly chose 20% of the samples for each species of *Stigmaphyllon*  
541 as validation and trained the model using the remainder for 30 epochs. Training was  
542 performed using all varKodes available for each sample (from 500kbp to 200Mbp). For  
543 validation, we separately evaluated whether each varKode with a different amount of data  
544 was correctly identified. For each replicate and amount of data used to validate varKodes,  
545 we recorded the average validation accuracy across the validation set. We then applied a  
546 linear model to predict the effect of all training parameters and amount of data in  
547 validation varKodes on the arc-sin transformed validation accuracy. We started from the  
548 full model containing all parameters and their interactions and reduced the model step-  
549 wise based on AIC scores, as implemented in the R function step.

550

551 *Testing sample number requirements*—A legitimate concern with complex neural networks  
552 is that they require vast amounts of training data and that typical skimming data sets might  
553 be insufficient for them to be useful. We tested the robustness of our models to the effect of  
554 the number of samples per species included in training by using from one to seven samples  
555 per species as training set and the remaining as validation, with 50 replicates per number  
556 of training samples. The batch size used in training was adjusted for the cases with very  
557 few samples included, so that each training epoch included about 10 batches. We included  
558 varKodes from 1Mbp to 200Mbp in both training and validation sets. In this case, we  
559 applied the training parameters informed by our previous analyses: a *resnext101*  
560 architecture, random initial weights, *CutMix* augmentation, and label smoothing for 30  
561 epochs. We visualized the effect of the number of samples by plotting the average  
562 validation accuracy of each sample against the number of training samples used in each  
563 case.

564

565 *Testing the effect of data quality*—Most of the cases with low accuracy corresponded to  
566 samples with low DNA yield (**Figure 2B**). We identified that DNA extraction yield was  
567 significantly correlated with two metrics of DNA quality: average insert size and variation  
568 in nucleotide composition along reads<sup>68</sup> (**Figure 4**). varKodes produced from these

569 samples may be visually distinct from other samples of the same species (**Figure 5**). For  
570 this reason, we further tested whether sample quality in training or validation impacted  
571 accuracy. Using both quality metrics, we identified the five lowest quality samples for each  
572 species. We next produced training sets using six randomly chosen samples per species,  
573 varying the number of low-quality samples included in training from zero to four. We  
574 included varKodes from 1Mbp to 200Mbp in both training and validation sets. We repeated  
575 this for 30 replicates for each number of low-quality samples. Like our tests with varying  
576 sample numbers, we applied the following training parameters: a *resnext101* architecture,  
577 random initial weights, *CutMix* augmentation, label smoothing for 30 epochs. For the  
578 validation set, we separately recorded the accuracy for high- and low-quality samples. We  
579 then visualized the effect of inclusion of low-quality samples in the training set by  
580 observing the distribution of validation accuracies for high-quality and low-quality samples  
581 across the range of number of low-quality samples included in the training set.

582

583 *Implementation of varKoder*—Following all of the tests described above, we implemented  
584 the optimal neural network training strategies in a python program named **varKoder**.  
585 *varKoder* can process, train and query varKodes and is freely available on our GitHub:  
586 <https://github.com/brunoasm/varKoder>. Because it employs standard neural network  
587 frameworks (namely, *pytorch*<sup>77</sup>, *fastai*<sup>78</sup>, and *timm*<sup>108</sup>), any of the image classification  
588 models and training hyperparameters available now or in the future via these libraries can  
589 be easily adapted and applied to varKode classification. For example, since our initial tests,  
590 we have identified that a vision-transformer architecture<sup>61</sup> outperforms convolutional  
591 neural networks in varKode classification. This was also observed in other computer-vision  
592 tasks<sup>111</sup>. Moreover, we have implemented a multi-label model as the default to increase  
593 robustness to low-quality varKodes with little diagnostic information in the training set.  
594 This was done by using an asymmetric multi-label loss function<sup>70</sup> instead of the standard  
595 cross-entropy loss function used in single-label classification. A vision-transformer  
596 architecture and multi-label classification are now default in *varKoder* v.0.8.0, which was  
597 used in all subsequent analyses.

598 **varKoder evaluation and comparison to alternatives**  
599 **using a de novo Malpighiales genomic dataset**

600 *varKoder*—To test *varKoder* performance in a complex dataset spanning multiple  
601 taxonomic levels and varying phylogenetic depths, we used the Malpighiales dataset  
602 including genera in Elatinaceae, Chrysobalanaceae and Malpighiaceae. Species of  
603 *Stigmaphyllon* (Malpighiaceae) were labeled with species, genus, and family names; all  
604 other samples were labeled with genus and family names. We tested the performance of  
605 *varKoder* in each sample with leave-one-out cross-validation. For each sample, we retained  
606 it as validation and trained a neural network using all of the other samples. In preliminary  
607 assessments, we found that a vision transformer architecture combined with a multi-label  
608 model sometimes led to instability in training for some datasets. For that reason, we used a  
609 two-step approach. Models were pre-trained for 20 epochs as single-label, using the least  
610 inclusive taxonomic assignment available for each sample and a base learning rate of 0.05.  
611 Next, we trained for an additional 10 epochs using the pre-trained weights but with a much  
612 smaller learning rate (0.005) and a multi-label output. Training samples included varKodes  
613 from 500 Kbp to 200 Mbp, and we recorded validation accuracy separately for varKodes  
614 produced from each amount of data. We used an arbitrary confidence threshold of 0.7 to  
615 make predictions in the multilabel models. For validation samples, we deemed a prediction  
616 correct if only the correct taxon was predicted for each taxonomic rank (i.e., species, genus,  
617 family). We deemed a prediction incorrect if one or more predictions passed the threshold  
618 for a taxonomic rank, but none match the actual label. When predicted labels included both  
619 the correct and incorrect taxa, we deemed it ambiguous. If the output prediction included  
620 no taxon with confidence above the threshold, we considered it as inconclusive. As metrics  
621 across all samples, we used prediction and recall, averaged across all predictions. We  
622 visualized the fraction of correct, incorrect, ambiguous, and inconclusive samples for each  
623 taxonomic rank and each amount of data used to produce varKodes.

624

625 *Skmer*—To compare *varKoder* with alternative methods, we used fastq files cleaned and  
626 subsampled by *varKoder* as input files to *Skmer*. In this case, we also used leave-one-out  
627 cross-validation to evaluate performance. For each amount of input data (500Kbp to

628 200Mbp), we cycled through all samples, constructing a *Skmer* database with the "*skmer*  
629 *reference*" command and including all samples but one. We then used the "*skmer query*"  
630 command on the sample left out and deemed the identification as correct if the sample in  
631 the reference database with closest estimated genetic distance had the correct taxon label.  
632 Because *Skmer* could always query a sample and there is no objective criterion to consider  
633 matches beyond the best match, the output predictions can only be correct or incorrect, but  
634 not inconclusive or ambiguous. We visualized the results similarly as we did with *varKoder*.  
635

636 *Conventional plant barcodes*—To infer phylogenies from our genome skim data (Figure 1),  
637 we applied the *PhyloHerb* bioinformatic pipeline<sup>112</sup>, which has been recently applied by a  
638 variety of projects from algae to flowering plants<sup>99, 101, 102</sup>. Briefly, this pipeline works as  
639 follows: for plastid loci, *PhyloHerb* maps raw short reads to a database of land plant plastid  
640 genomes. Mapped reads are then assembled into scaffolds using *SPAdes*<sup>113</sup> and plastid loci  
641 are identified using nucleotide BLAST searches with a default e-value threshold of 1e-40.  
642 *PhyloHerb* then outputs orthologous plastid genes into individual FASTA files, which are fed  
643 directly into MAFFT v7.407<sup>114</sup> for alignment. Alignments are then concatenated into a  
644 super matrix using the 'conc' function within the *PhyloHerb* package. Phylogenies for both  
645 individual locus and the concatenated alignment were inferred with IQTREE v2.0.6 using  
646 the GTR+GAMMA model with 1000 ultrafast bootstrap replicates<sup>115</sup>.

647 To recover the traditional plant barcodes, *rbcl*, *matK*, *trnL-F*, *ndhF*, and ITS, from our  
648 Malpighiales genome skim data, we applied GetOrganelle v1.7.7.0<sup>116</sup> and *PhyloHerb*  
649 v1.1.1<sup>112</sup> to automatically assemble and extract these DNA markers, respectively. Briefly,  
650 the complete or subsampled genome skim data were first assembled into plastid genomes  
651 or nuclear ribosomal regions using *GetOrganelle*<sup>116</sup> with its default settings. Next,  
652 *PhyloHerb* was applied to extract the relevant barcode genes using its built-in BLAST  
653 database. To test whether these traditional barcodes provided accurate identification to  
654 species, genus, and family, we ran an all-by-all BLASTn analysis for each individual gene  
655 across the same data subsampling schemes as *Skmer* and *varKoder*. BLAST targets were  
656 always drawn from assemblies using all the data available for each specimen, whereas  
657 queries included assemblies from input data amounts varying from 500 Kbp to 200 Mbp.

658 Within each BLAST analysis for each one of the Malpighiales accessions, we deemed an  
659 identification to be correct if the best non-self BLAST hit came from the same taxon, and  
660 incorrect otherwise. We deemed it inconclusive if the locus could not be assembled for that  
661 amount of data or BLAST returned no results. For concatenated barcodes, we produced a  
662 phylogenetic tree for each amount of data, and deemed an identification to be correct if the  
663 sample with lowest patristic distance came from the same taxon. We deemed it to be  
664 inconclusive when none of the genes in the concatenated dataset could be assembled for a  
665 sample. We visualized results similarly to *varKoder*, separately for each conventional  
666 barcoding gene and for the concatenated dataset.

667

### 668 **varKoder application in diverse published datasets**

669 *Species-level identification in plants, animals, fungi, and bacteria*—For each of the four  
670 organismal clades, we trained a multi-label model that included five species with at least  
671 three samples per species. For *Bembidion*, we included five species with five samples per  
672 species. For *Corallorhiza*, we included five species (or varieties) with at least five samples  
673 per species, except for *C. striata* var. *vreelandii* and *C. striata* var. *striata*, for which we  
674 included six and seven samples each, respectively. For *Mycobacterium tuberculosis*, we  
675 included representatives of five monophyletic *M. tuberculosis* lineages (L1, L2, L3,  
676 L4.1.i1.2.1, and L4.3.i2) with seven clinical isolates per lineage. Samples for *Bembidion*,  
677 *Corallorhiza*, and *M. tuberculosis* isolates all formed monophyletic groups, whereas  
678 *Xanthoparmelia* species did not. Since the *Xanthoparmelia* species were paraphyletic, we  
679 subsampled only monophyletic groups for model training. In this case, four species  
680 included three samples per species (*X. camtschadalis*, *X. mexicana*, *X. neocumberlandia*, and  
681 *X. coloradoensis*) and one species included five samples per species (*X. chlorochroa*). One  
682 potential confounding factor for the *Xanthoparmelia* model is that *Xanthoparmelia* is a  
683 lichen-forming fungus and thus genome skim data represents a chimera of fungal and algal  
684 genomes representing both partners in this unique symbiosis. Species of the algal symbiont  
685 *Trebouxia* are flexible generalists across fungal species *Xanthoparmelia*. Since these  
686 genome skims are a mix of both algal photobiont and fungus, we hypothesize the accuracy  
687 of our model decreased because of the more generalist nature of *Trebouxia*<sup>117</sup>.

688 For all four test cases, we applied default *varKoder* v.0.8.0 parameters for generating  
689 varKode images, training each model, and testing the accuracy of the trained model using  
690 the ‘query’ function. In all cases, we included all the available data for each training or  
691 validation sample. To test if trained models accurately predicted species identity, we  
692 queried them using genome skim samples not used for training but from the same species  
693 included in the model. We also tested genome skim samples of species within the same  
694 genus but not used in model training. As in the case of Malpighiales, we set the threshold to  
695 make a prediction to 0.7 and used the same criteria to consider a prediction correct,  
696 incorrect, inconclusive, or ambiguous. We separately evaluated results for taxa with  
697 representatives included in the training set and taxa used only as queries, without  
698 conspecific samples in the training set.

699

700 *All eukaryotic families data set from SRA*—Each accession obtained from SRA was labeled  
701 with its family identification obtained from NCBI. Because of the larger size of this dataset,  
702 a leave-one-out cross-validation approach would have been intractable. Therefore, we  
703 randomly selected 80% of the samples in each family as the training set and used the  
704 remainder for validation. Similarly to Malpighiales, we used a two-step training method by  
705 pre-training as a single-label model and finalizing with a multi-label model. However,  
706 because of the larger size of this dataset, we adjusted the base learning rate and batch size  
707 to accelerate training. Namely, pre-training was done with a learning rate of 0.1 and a batch  
708 size of 300 for 30 epochs. Final training was done with the same batch size but a smaller  
709 base learning rate of 0.01 in 5 epochs with frozen body weights and three epochs with  
710 unfrozen weights.

711

## 712 **Acknowledgements**

713 BdM received postdoctoral fellowships from the Harvard University Museum of  
714 Comparative Zoology and the Smithsonian Tropical Research Institute during the early  
715 stages of this study. LC was supported by Harvard University and by a Stengl Wyer  
716 scholarship from the University of Texas at Austin. PF was supported by LVMH Research,  
717 and Dior Science. YY was supported by a postdoctoral fellowship from Harvard University  
718 Herbaria. CCD was supported by Harvard University, LVMH Research, Dior Science, and  
719 National Science Foundation grants DEB-1355064 and DEB-0544039. Computations were  
720 performed at the Harvard Cannon Cluster and the Field Museum Grainger Bioinformatics  
721 Center. We thank the Bauer Core Facility, and especially Claire Reardon, at Harvard  
722 University for providing technical support during the laboratory process. We thank R.  
723 Asprino and K. Peterson for their assistance and the team at Sound Solutions for  
724 Sustainable Science for carefully editing early versions of our manuscript.

## 725 **Author contributions**

726 BdM conceived varKodes and wrote the program *varKoder*. BdM and CCD designed the  
727 research. CCD, XD, YY, LCM, and CA collected the new sequence data. BdM, CCD, LC, YY, PJF  
728 analyzed and interpreted the data. LCM prepared the figures. BdM and CCD wrote the  
729 manuscript with key contributions from LC, YY and PJF. All authors approved the  
730 manuscript.

## 731 **Code Availability**

732 The current version of varKoder is available at <https://github.com/brunoasm/varKoder>. A  
733 fastai model pre-trained on SRA data is available at  
734 [https://huggingface.co/brunoasm/vit\\_large\\_patch32\\_224.NCBI\\_SRA](https://huggingface.co/brunoasm/vit_large_patch32_224.NCBI_SRA)

735  
736  
737  
738  
739  
740  
741  
742  
743  
744  
745  
746  
747  
748  
749  
750  
751  
752  
753  
754  
755  
756  
757  
758  
759  
760  
761  
762  
763  
764  
765  
766  
767  
768  
769  
770  
771  
772  
773  
774  
775  
776  
777  
778

## References

1. Hebert PDN, Ratnasingham S, de Waard JR. Barcoding animal life: cytochrome c oxidase subunit 1 divergences among closely related species. *Proc Royal Soc B* **270**, S96-S99 (2003).
2. Kress WJ. Plant DNA barcodes: applications today and in the future. *J Syst Evol* **55**, 291-307 (2017).
3. Ratnasingham S, Hebert PDN. BOLD: The Barcode of Life Data System (<http://www.barcodinglife.org>). *Mol Ecol Notes* **7**, 355-364 (2007).
4. Taberlet P, Coissac E, Pompanon F, Brochmann C, Willerslev E. Towards next-generation biodiversity assessment using DNA metabarcoding. *Mol Ecol* **21**, 2045-2050 (2012).
5. Seifert KA. Progress towards DNA barcoding of fungi. *Mol Ecol Res* **9 Suppl s1**, 83-89 (2009).
6. Sharkey MJ, *et al.* Minimalist revision and description of 403 new species in 11 subfamilies of Costa Rican braconid parasitoid wasps, including host records for 219 species. *Zookeys* **1013**, 1-665 (2021).
7. Lahaye R, *et al.* DNA barcoding the floras of biodiversity hotspots. *Proc Natl Acad Sci USA*, 0709936105 (2008).
8. Kuzmina ML, *et al.* Using herbarium-derived DNAs to assemble a large-scale DNA barcode library for the vascular plants of Canada. *Appl Plant Sci* **5**, apps.1700079 (2017).
9. Muñoz-Rodríguez P, *et al.* A taxonomic monograph of *Ipomoea* integrated across phylogenetic scales. *Nat Plants* **5**, 1136-1144 (2019).
10. Hebert PD, Penton EH, Burns JM, Janzen DH, Hallwachs W. Ten species in one: DNA barcoding reveals cryptic species in the neotropical skipper butterfly *Astraptes fulgerator*. *Proc Natl Acad Sci USA*, (2004).
11. Zeale MR, Butlin RK, Barker GL, Lees DC, Jones G. Taxon-specific PCR for DNA barcoding arthropod prey in bat faeces. *Mol Ecol Res* **11**, 236-244 (2011).
12. Nitta JH, Meyer JY, Taputuarai R, Davis CC. Life cycle matters: DNA barcoding reveals contrasting community structure between fern sporophytes and gametophytes. *Ecol Monograph* **87**, 278-296 (2016).

- 779  
780 13. Kress WJ, *et al.* Plant DNA barcodes and a community phylogeny of a tropical forest  
781 dynamics plot in Panama. *Proc Natl Acad Sci USA* **106**, 18621-18626 (2009).  
782
- 783 14. Willis CG, Franzone BF, Xi Z, Davis CC. The establishment of Central American  
784 migratory corridors and the biogeographic origins of seasonally dry tropical forests  
785 in Mexico. *Front Genet* **5**, 433 (2014).  
786
- 787 15. Willerslev E, *et al.* Ancient biomolecules from deep ice cores reveal a forested  
788 Southern Greenland. *Science* **317**, 111-114 (2007).  
789
- 790 16. Crump SE, *et al.* Ancient plant DNA reveals High Arctic greening during the Last  
791 Interglacial. *Proc Natl Acad Sci USA* **118**, e2019069118 (2021).  
792
- 793 17. Kjær KH, *et al.* A 2-million-year-old ecosystem in Greenland uncovered by  
794 environmental DNA. *Nature* **612**, 283-291 (2022).  
795
- 796 18. Fierer N, Lauber CL, Zhou N, McDonald D, Costello EK, Knight R. Forensic  
797 identification using skin bacterial communities. *Proc Natl Acad Sci USA* **107**, 6477-  
798 6481 (2010).  
799
- 800 19. Rollo F, Ubaldi M, Ermini L, Marota I. Ötzi's last meals: DNA analysis of the intestinal  
801 content of the Neolithic glacier mummy from the Alps. *Proc Natl Acad Sci USA* **99**,  
802 12594-12599 (2002).  
803
- 804 20. Yu J, Wu X, Liu C, Newmaster S, Ragupathy S, Kress WJ. Progress in the use of DNA  
805 barcodes in the identification and classification of medicinal plants. *Ecotoxicol*  
806 *Environ Saf* **208**, 111691 (2021).  
807
- 808 21. Ashfaq M, Hebert PDN. DNA barcodes for bio-surveillance: regulated and  
809 economically important arthropod plant pests. *Genome* **59**, 933-945 (2016).  
810
- 811 22. Eaton MJ, Meyers GL, Kolokotronis S-O, Leslie MS, Martin AP, Amato G. Barcoding  
812 bushmeat: molecular identification of Central African and South American harvested  
813 vertebrates. *Conserv Genet* **11**, 1389-1404 (2010).  
814
- 815 23. Liu J, *et al.* Integrating a comprehensive DNA barcode reference library with a global  
816 map of yews (*Taxus* L.) for forensic identification. *Mol Ecol Res* **18**, 1115-1131  
817 (2018).  
818
- 819 24. Ogden R, Dawnay N, McEwing R. Wildlife DNA forensics—bridging the gap between  
820 conservation genetics and law enforcement. *Endanger Species Res* **9**, 179-195  
821 (2009).  
822

- 823 25. Williamson J, *et al.* Exposing the illegal trade in cycad species (Cycadophyta:  
824 *Encephalartos*) at two traditional medicine markets in South Africa using DNA  
825 barcoding. *Genome* **59**, 771-781 (2016).  
826
- 827 26. Costa FO, Carvalho GR. The Barcode of Life Initiative: synopsis and prospective  
828 societal impacts of DNA barcoding of Fish. *Genomics, Society and Policy* **3**, 29 (2007).  
829
- 830 27. Gao Z, Liu Y, Wang X, Wei X, Han J. DNA mini-barcoding: a derived barcoding method  
831 for herbal molecular identification. *Front Plant Sci* **10**, (2019).  
832
- 833 28. Molina J, *et al.* Possible loss of the chloroplast genome in the parasitic flowering  
834 plant *Rafflesia lagascae* (Rafflesiaceae). *Mol Biol Evol* **31**, 793-803 (2014).  
835
- 836 29. Cai L, *et al.* Deeply altered genome architecture in the endoparasitic flowering plant  
837 *Sapria himalayana* Griff. (Rafflesiaceae). *Curr Biol* **31**, 1002-1011.e1009 (2021).  
838
- 839 30. Richardson JE, Pennington RT, Pennington TD, Hollingsworth PM. Rapid  
840 diversification of a species-rich genus of neotropical rain forest trees. *Science* **293**,  
841 2242-2245 (2001).  
842
- 843 31. Wang J, Luo J, Ma Y-Z, Mao X-X, Liu J-Q. Nuclear simple sequence repeat markers are  
844 superior to DNA barcodes for identification of closely related *Rhododendron* species  
845 on the same mountain. *J Syst Evol* **57**, 278-286 (2019).  
846
- 847 32. Su X, Wu G, Li L, Liu J. Species delimitation in plants using the Qinghai-Tibet Plateau  
848 endemic *Orinus* (Poaceae: Tridentinae) as an example. *Ann Bot* **116**, 35-48 (2015).  
849
- 850 33. Lu Z, Sun Y, Li Y, Yang Y, Wang G, Liu J. Species delimitation and hybridization  
851 history of a hazel species complex. *Ann Bot* **127**, 875-886 (2021).  
852
- 853 34. Cai L, *et al.* The perfect storm: gene tree estimation error, incomplete lineage  
854 sorting, and ancient gene flow explain the most recalcitrant ancient angiosperm  
855 clade, Malpighiales. *Syst Biol* **70**, 491-507 (2021).  
856
- 857 35. Clarke LJ, Soubrier J, Weyrich LS, Cooper A. Environmental metabarcodes for  
858 insects: in silico PCR reveals potential for taxonomic bias. *Mol Ecol Res* **14**, 1160-  
859 1170 (2014).  
860
- 861 36. Song H, Buhay JE, Whiting MF, Crandall KA. Many species in one: DNA barcoding  
862 overestimates the number of species when nuclear mitochondrial pseudogenes are  
863 coamplified. *Proc Natl Acad Sci USA* **105**, 13486-13491 (2008).  
864
- 865 37. Xiong H, *et al.* Species tree estimation and the impact of gene loss following whole-  
866 genome duplication. *Syst Biol* **71**, 1348-1361 (2022).  
867

- 868 38. Straub SCK, Parks M, Weitemier K, Fishbein M, Cronn RC, Liston A. Navigating the tip  
869 of the genomic iceberg: Next-generation sequencing for plant systematics. *Amer J*  
870 *Bot* **99**, 349-364 (2012).  
871
- 872 39. Bohmann K, Mirarab S, Bafna V, Gilbert MTP. Beyond DNA barcoding: The  
873 unrealized potential of genome skim data in sample identification. *Mol Ecol* **29**,  
874 2521-2534 (2020).  
875
- 876 40. Sarmashghi S, Bohmann K, P. Gilbert MT, Bafna V, Mirarab S. Skmer: assembly-free  
877 and alignment-free sample identification using genome skims. *Genome Biol* **20**, 34  
878 (2019).  
879
- 880 41. Borowiec ML, Dikow RB, Frandsen PB, McKeeken A, Valentini G, White AE. Deep  
881 learning as a tool for ecology and evolution. *Methods Ecol Evol* **13**, 1640-1660  
882 (2022).  
883
- 884 42. Millán Arias P, Alipour F, Hill KA, Kari L. DeLUCS: Deep learning for unsupervised  
885 clustering of DNA sequences. *PLOS ONE* **17**, e0261531 (2022).  
886
- 887 43. Kari L, *et al.* Mapping the space of genomic signatures. *PLOS ONE* **10**, e0119815  
888 (2015).  
889
- 890 44. Fiannaca A, *et al.* Deep learning models for bacteria taxonomic classification of  
891 metagenomic data. *BMC Bioinform* **19**, 198 (2018).  
892
- 893 45. Linard B, Swenson K, Pardi F. Rapid alignment-free phylogenetic identification of  
894 metagenomic sequences. *Bioinform* **35**, 3303-3312 (2019).  
895
- 896 46. Desai HP, Parameshwaran AP, Sunderraman R, Weeks M. Comparative study using  
897 neural networks for 16S ribosomal gene classification. *J Comput Biol* **27**, 248-258  
898 (2020).  
899
- 900 47. Shang J, Sun Y. CHEER: HierarCHical taxonomic classification for viral mEtagEnomic  
901 data via deep leaRning. *Methods* **189**, 95-103 (2021).  
902
- 903 48. LeCun Y, Bengio Y, Hinton G. Deep learning. *Nature* **521**, 436-444 (2015).  
904
- 905 49. Cong Y, Ye X, Mei Y, He K, Li F. Transposons and non-coding regions drive the  
906 intrafamily differences of genome size in insects. *iScience* **25**, 104873 (2022).  
907
- 908 50. Heckenhauer J, *et al.* Genome size evolution in the diverse insect order Trichoptera.  
909 *GigaScience* **11**, giac011 (2022).  
910
- 911 51. Schley RJ, *et al.* The ecology of palm genomes: repeat-associated genome size  
912 expansion is constrained by aridity. *New Phytol* **236**, 433-446 (2022).

- 913  
914 52. Sproul JS, Barton LM, Maddison DR. Repetitive DNA profiles reveal evidence of rapid  
915 genome evolution and reflect species boundaries in ground beetles. *Syst Biol*,  
916 (2020).  
917
- 918 53. Jeffrey HJ. Chaos game representation of gene structure. *Nucleic Acids Res* **18**, 2163-  
919 2170 (1990).  
920
- 921 54. Davis CC, Anderson WR. A complete generic phylogeny of Malpighiaceae inferred  
922 from nucleotide sequence data and morphology. *Amer J Bot* **97**, 2031-2048 (2010).  
923
- 924 55. Cai L, Xi Z, Peterson K, Rushworth C, Beaulieu J, Davis CC. Phylogeny of Elatinaceae  
925 and the tropical Gondwanan origin of the Centroplacaceae (Malpighiaceae,  
926 Elatinaceae) clade. *PLOS ONE* **11**, e0161881 (2016).  
927
- 928 56. Davis CC, Anderson WR, Donoghue MJ. Phylogeny of Malpighiaceae: evidence from  
929 chloroplast *ndhF* and *trnL-F* nucleotide sequences. *Amer J Bot* **88**, 1830-1846  
930 (2001).  
931
- 932 57. Anderson C. Revision of *Ryssopterys* and transfer to *Stigmaphyllon* (Malpighiaceae).  
933 *Blumea* **56**, 73–104 (2011).  
934
- 935 58. Anderson C. Monograph of *Stigmaphyllon* (Malpighiaceae). *Syst Bot Monogr* **51**, 1-  
936 313 (1997).  
937
- 938 59. Christin S, Hervet É, Lecomte N. Applications for deep learning in ecology. *Methods*  
939 *Ecol Evol* **10**, 1632-1644 (2019).  
940
- 941 60. He T, Zhang Z, Zhang H, Zhang Z, Xie J, Li M. Bag of tricks for image classification  
942 with convolutional neural networks. *arXiv*, (2018).  
943
- 944 61. Vaswani A, *et al.* Attention is all you need. (2017).  
945
- 946 62. Szegedy C, Vanhoucke V, Ioffe S, Shlens J, Wojna Z. Rethinking the inception  
947 architecture for computer vision. In: *2016 IEEE Conference on Computer Vision and*  
948 *Pattern Recognition (CVPR)* (2016).  
949
- 950 63. Smith LN. A disciplined approach to neural network hyper-parameters: Part 1 --  
951 learning rate, batch size, momentum, and weight decay. *arXiv*, (2018).  
952
- 953 64. Zhang H, Cisse M, Dauphin YN, Lopez-Paz D. mixup: beyond empirical risk  
954 minimization. *arXiv*, (2018).  
955
- 956 65. Yun S, Han D, Oh SJ, Chun S, Choe J, Yoo Y. CutMix: regularization strategy to train  
957 strong classifiers with localizable features. *arXiv*, (2019).

958  
959 66. Xie S, Girshick R, Dollár P, Tu Z, He K. Aggregated residual transformations for deep  
960 neural networks. *arXiv* **1611.05431**, (2017).  
961  
962 67. Goodfellow I. *Deep learning*. The MIT Press (2016).  
963  
964 68. Weiß CL, *et al.* Temporal patterns of damage and decay kinetics of DNA retrieved  
965 from plant herbarium specimens. *R Soc Open Sci* **3**, 160239 (2016).  
966  
967 69. Rachtman E, Balaban M, Bafna V, Mirarab S. The impact of contaminants on the  
968 accuracy of genome skimming and the effectiveness of exclusion read filters. *Mol*  
969 *Ecol Res* **20**, 649-661 (2020).  
970  
971 70. Ben-Baruch E, *et al.* Asymmetric loss for multi-label classification. *arXiv*, (2021).  
972  
973 71. Bushnell B. BBMap.). <https://sourceforge.net/projects/bbmap/> (2022).  
974  
975 72. Bushnell B, Rood J, Singer E. BBMerge – Accurate paired shotgun read merging via  
976 overlap. *PLOS ONE* **12**, e0185056 (2017).  
977  
978 73. Rizk G, Lavenier D, Chikhi R. DSK: k-mer counting with very low memory usage.  
979 *Bioinform* **29**, 652-653 (2013).  
980  
981 74. Chen S, Zhou Y, Chen Y, Gu J. fastp: an ultra-fast all-in-one FASTQ preprocessor.  
982 *Bioinform* **34**, i884-i890 (2018).  
983  
984 75. Tange O. *GNU Parallel 2018*. Ole Tange (2018).  
985  
986 76. Harris CR, *et al.* Array programming with NumPy. *Nature* **585**, 357-362 (2020).  
987  
988 77. Paszke A, *et al.* PyTorch: an imperative style, high-performance deep learning  
989 library. In: *Advances in Neural Information Processing Systems 32*. Curran  
990 Associates, Inc. (2019).  
991  
992 78. Howard J, Gugger S. Fastai: a layered API for deep learning. *Information* **11**, 108  
993 (2020).  
994  
995 79. Pellicer J, Leitch IJ. The Plant DNA C-values database (release 7.1): an updated  
996 online repository of plant genome size data for comparative studies. *New Phytol*  
997 **226**, 301-305 (2020).  
998  
999 80. D’Ercole J, Prosser SWJ, Hebert PDN. A SMRT approach for targeted amplicon  
1000 sequencing of museum specimens (Lepidoptera)—patterns of nucleotide  
1001 misincorporation. *PeerJ* **9**, e10420 (2021).  
1002

- 1003 81. Sproul JS, Barton LM, Maddison DR. Repetitive DNA profiles reveal evidence of rapid  
1004 genome evolution and reflect species boundaries in ground beetles. *Syst Biol* **69**,  
1005 1137-1148 (2020).  
1006
- 1007 82. Sproul JS, Maddison DR. Cryptic species in the mountaintops: species delimitation  
1008 and taxonomy of the *Bembidion* breve species group (Coleoptera: Carabidae) aided  
1009 by genomic architecture of a century-old type specimen. *Zool J Linn Soc* **183**, 556-  
1010 583 (2018).  
1011
- 1012 83. Keuler R, *et al.* Interpreting phylogenetic conflict: hybridization in the most speciose  
1013 genus of lichen-forming fungi. *Mol Phylog Evol* **174**, 107543 (2022).  
1014
- 1015 84. Barrett CF, Wicke S, Sass C. Dense infraspecific sampling reveals rapid and  
1016 independent trajectories of plastome degradation in a heterotrophic orchid  
1017 complex. *New Phytol* **218**, 1192-1204 (2018).  
1018
- 1019 85. Freschi L, *et al.* Population structure, biogeography and transmissibility of  
1020 *Mycobacterium tuberculosis*. *Nat Commun* **12**, 6099 (2021).  
1021
- 1022 86. Kimura LT, *et al.* Amazon Biobank: a collaborative genetic database for bioeconomy  
1023 development. *Funct Integr Genomics* **23**, 101 (2023).  
1024
- 1025 87. Cameron KM, Chase MW, Anderson WR, Hills HG. Molecular systematics of  
1026 Malpighiaceae: evidence from plastid *rbcl* and *matK* sequences. *Amer J Bot* **88**,  
1027 1847-1862 (2001).  
1028
- 1029 88. Anderson WR. Chromosome numbers of neotropical Malpighiaceae. *Contr Univ*  
1030 *Michigan Herb* **19**, 341-354 (1993).  
1031
- 1032 89. Ebenezer TE, *et al.* Africa: sequence 100,000 species to safeguard biodiversity.  
1033 *Nature* **603**, 388-392 (2022).  
1034
- 1035 90. Lewin HA, *et al.* The Earth BioGenome Project 2020: starting the clock. *Proc Natl*  
1036 *Acad Sci USA* **119**, e2115635118 (2022).  
1037
- 1038 91. Cheng S, *et al.* 10KP: A phylodiverse genome sequencing plan. *GigaScience* **7**, giy013  
1039 (2018).  
1040
- 1041 92. Staff E. A reference standard for genome biology. *Nat Biotechnol* **36**, 1121-1121  
1042 (2018).  
1043
- 1044 93. Davis CC. The herbarium of the future. *Trends Ecol Evol* **38**, 412-423 (2023).  
1045
- 1046 94. Davis CC. Collections are truly priceless. *Science* **383**, 1035-1035 (2024).  
1047

- 1048 95. Davis CC, Sessa EB, Paton A, Antonelli A, Teisher J. The destructive sampling  
1049 conundrum and guidelines for effective and ethical sampling of herbaria.  
1050 *EcoEvoRxiv*, (2024).  
1051
- 1052 96. Card DC, Shapiro B, Giribet G, Moritz C, Edwards SV. Museum genomics. *Annu Rev*  
1053 *Genet* **55**, 633-659 (2021).  
1054
- 1055 97. Davis CC. The herbarium of the future. *Trends Ecol Evol*, (2022).  
1056
- 1057 98. Lynch M. *The origins of genome architecture*. Sinauer Associates (2007).  
1058
- 1059 99. Marinho LC, *et al*. Plastomes resolve generic limits within tribe Clusieae (Clusiaceae)  
1060 and reveal the new genus Arawakia. *Mol Phylog Evol* **134**, 142-151 (2019).  
1061
- 1062 100. Weitemier K, *et al*. Hyb-Seq: combining target enrichment and genome skimming for  
1063 plant phylogenomics. *Appl Plant Sci* **2**, 1400042 (2014).  
1064
- 1065 101. Lucas MC, *et al*. Phylogenetic relationships of *Tovomita* (Clusiaceae): carpel number  
1066 and geographic distribution speak louder than venation pattern. *Syst Bot* **46**, 102-  
1067 108 (2021).  
1068
- 1069 102. Lyra GdM, *et al*. Phylogenomics, divergence time estimation and trait evolution  
1070 provide a new look into the Gracilariales (Rhodophyta). *Mol Phylog Evol* **165**,  
1071 107294 (2021).  
1072
- 1073 103. Yan Y, Davis CC, Dimitrov D, Wang Z, Rahbek C, Borregaard MK. Phylogeographic  
1074 history of the tea family inferred through high-resolution phylogeny and fossils. *Syst*  
1075 *Biol* **70**, 1256-1271 (2021).  
1076
- 1077 104. Sabin S, *et al*. A seventeenth-century *Mycobacterium tuberculosis* genome supports a  
1078 Neolithic emergence of the *Mycobacterium tuberculosis* complex. *Genome Biol* **21**,  
1079 201 (2020).  
1080
- 1081 105. Bushnell B. BBtools v.37.61.) (2017).  
1082
- 1083 106. van der Maaten L, Hinton G. Visualizing data using t-SNE. *JMLR* **9**, 2579-2605 (2008).  
1084
- 1085 107. Clark A. Pillow, Version 9.4.0. Software. <https://pypi.org/project/Pillow/>. (2023).  
1086
- 1087 108. Wightman R. PyTorch Image Models. (2019).  
1088
- 1089 109. He K, Zhang X, Ren S, Sun J. Deep residual learning for image recognition. *arXiv*  
1090 **1512.03385**, 1512.03385-01512.03385 (2015).  
1091

- 1092 110. Tan M, Le QV. EfficientNet: rethinking model scaling for convolutional neural  
1093 networks. *arXiv*, abs/1905.11946 (2019).  
1094
- 1095 111. Dosovitskiy A, *et al.* An image is worth 16x16 words: transformers for image  
1096 recognition at scale. *arXiv*, (2020).  
1097
- 1098 112. Cai L, Zhang H, Davis CC. PhyloHerb: A high-throughput phylogenomic pipeline for  
1099 processing genome skimming data. *Appl Plant Sci* **10**, e11475 (2022).  
1100
- 1101 113. Bankevich A, *et al.* SPAdes: a new genome assembly algorithm and Its applications  
1102 to single-cell sequencing. *J Comput Biol* **19**, 455-477 (2012).  
1103
- 1104 114. Katoh K, Standley DM. MAFFT multiple sequence alignment software version 7:  
1105 improvements in performance and usability. *Mol Biol Evol* **30**, 772-780 (2013).  
1106
- 1107 115. Minh BQ, *et al.* IQ-TREE 2: New Models and Efficient Methods for Phylogenetic  
1108 Inference in the Genomic Era. *Mol Biol Evol* **37**, 1530-1534 (2020).  
1109
- 1110 116. Jin J-J, *et al.* GetOrganelle: a fast and versatile toolkit for accurate de novo assembly  
1111 of organelle genomes. *Genome Biol* **21**, 241 (2020).  
1112
- 1113 117. Leavitt SD, *et al.* Fungal specificity and selectivity for algae play a major role in  
1114 determining lichen partnerships across diverse ecogeographic regions in the lichen-  
1115 forming family Parmeliaceae (Ascomycota). *Mol Ecol* **24**, 3779-3797 (2015).  
1116  
1117